



## EXPERIMENTAL STUDY ON SHEAR BEHAVIOR OF HOLLOW PRECAST STEEL-ENCASED HIGH-STRENGTH SPUN CONCRETE PILES

T. Obara<sup>(1)</sup>, M. Egawa<sup>(2)</sup>, S. Thusoo<sup>(3)</sup>, S. Kono<sup>(4)</sup>, K. Miyahara<sup>(5)</sup>, D. Mukai<sup>(6)</sup>

<sup>(1)</sup> Assistant Professor, Institute of Innovative Research, Tokyo Institute of Technology, [obara.t.ac@m.titech.ac.jp](mailto:obara.t.ac@m.titech.ac.jp)

<sup>(2)</sup> Graduate Student, Dept. of Civil and Environmental Engineering, Tokyo Institute of Technology, [egawa.m.ab@m.titech.ac.jp](mailto:egawa.m.ab@m.titech.ac.jp)

<sup>(3)</sup> Graduate Student, Dept. of Architecture and Building Engineering, Tokyo Institute of Technology, [thusoo.s.aa@m.titech.ac.jp](mailto:thusoo.s.aa@m.titech.ac.jp)

<sup>(4)</sup> Professor, Institute of Innovative Research, Tokyo Institute of Technology, [kono.s.ae@m.titech.ac.jp](mailto:kono.s.ae@m.titech.ac.jp)

<sup>(5)</sup> Engineer, Concrete Pile and Pole Industrial Technology Association, [copita\\_a@c-pile.or.jp](mailto:copita_a@c-pile.or.jp)

<sup>(6)</sup> Associate Professor, Dept. of Civil and Architectural Engineering, University of Wyoming, [dmukai@uwyo.edu](mailto:dmukai@uwyo.edu)

...

### Abstract

In the 2011 Tohoku earthquake and the 2016 Kumamoto earthquake, some buildings were demolished because of damages to precast concrete piles near the pile head. In Japan, superstructures are designed using working stress design for intermediate earthquakes and a lateral load carrying capacity check for severe earthquakes. However, substructures are not required to be designed for severe earthquakes and the structural performance of piles in terms of moment capacity, shear capacity, and ductility after yielding of members is not clear. For better seismic performance, hollow precast steel-encased high-strength spun concrete piles (SC piles) are often used at the pile head in low and mid-rise buildings in Japan. Extensive research works have been conducted recently to study the flexural performance of SC piles i.e. moment capacity and ultimate deformation. However, in addition to large moment, the pile head is also subject to large shear force during an earthquake and it is equally important to understand the shear behavior of piles. The standard WG final report by Building Research Institute (BRI) regarding pile foundations (hereafter, the 2000 BRI report) provides an equation to estimate shear capacity of SC piles. However, the accuracy of this equation and shear behavior of piles with and without axial loads has not been definitively confirmed. According to the 2000 BRI report, shear capacity is calculated by considering the contribution of the steel casing only while moment capacity is calculated by considering the contribution of both steel casing and concrete. In this paper, a revised equation for shear capacity including concrete contribution is used to reproduce the experimental results.

The current project involves testing of a precast steel-encased high-strength spun concrete pile specimens (SCS1). This paper describes the results from testing of the specimens which were tested to evaluate shear behavior, especially the shear ultimate capacity. Based on the equations in the 2000 BRI report, the shear to moment capacity ratio was small enough to have shear failure. The specimens had an external diameter of 400 mm, steel casing thickness of 6 mm and concrete thickness of about 80 mm. Static loading was applied under antisymmetric moment condition while keeping a constant axial force ratio of 0.1 (1000 kN) (positive values are compressive force and negative values are tensile force.).

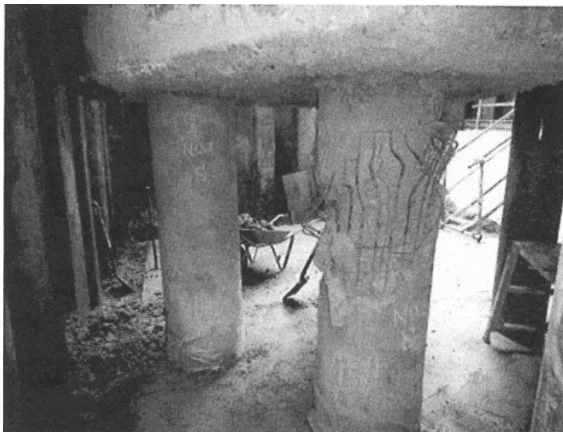
SCS1 showed high shear force capacity and ductility in the experiment. The maximum lateral force capacity reached 2030 kN at a drift ratio(R) of 2.4% and the ultimate drift at which moment capacity dropped by 20% of maximum moment capacity was 6.0%. The steel casing yielded in shear at  $R=1.14\%$  after flexural yielding in tension and compression. It was observed that the steel casing buckled locally near the base of the pile at maximum moment capacity. The failure mode was established to be flexure caused by local buckling. Shear maximum capacity in the experiment was compared with three equations of shear ultimate capacity and a flexural capacity based on a fiber model. To further understand the shear behavior of SC piles, the shear resistance mechanism is clarified from the experimental results and shear related information is summarized in order to improve performance based design for SC piles.

*Keywords: Precast pile, High-strength concrete, Hollow spun pile, Shear behavior, Buckling of steel*



## 1. Introduction

In the 2011 Tohoku earthquake and 2016 Kumamoto earthquake, some buildings suffered damage to precast concrete piles near the pile head (Photo 1) [1, 2]. In Japan, superstructures are designed using working stress design for intermediate earthquakes and load carrying capacity checks are carried out for severe earthquakes. However, substructures are not required to be designed for severe earthquakes and the structural performance of piles in terms of moment capacity, shear capacity, and ductility after yielding of members is not clear. For better seismic performance, hollow precast steel-encased high-strength spun concrete piles (SC piles) are often used at pile heads in low and mid-rise buildings in Japan. Extensive research works have been conducted recently to study the flexural performance of SC piles, i.e. moment capacity and ultimate deformation [3, 4]. However, in addition to a large moment, the pile heads are also subject to large shear force during an earthquake and it is equally important to understand the shear maximum capacity and shear behavior. The standard WG final report by Building Research Institute (BRI) regarding pile foundations (hereafter, the 2000 BRI report) provides an equation to estimate shear maximum capacity of SC piles (Eq. (1)) [5]. However, the accuracy of this equation and shear behavior of SC piles with and without axial loads has not been definitively confirmed because this equation was developed for concrete-filled steel tube piles. According to Eq. (1) in the 2000 BRI report, although shear capacity is calculated by considering the contribution of steel casing when the shear stress of steel casing reaches the shear strength (Eq. (2)), the contribution of concrete shear strength is based on the ratio of steel to concrete moment capacity. Therefore, at present, the effect of concrete contribution to shear capacity is not clear. In this paper, shear behavior of SC piles is made clearer from the experimental results and a revised equation for shear capacity with concrete contribution is used to reproduce the experimental results.



(a) The 2011 Tohoku earthquake



(b) The 2016 Kumamoto earthquake

Photo 1 – Damage of concrete piles in the earthquakes [1, 2]

$$Q_{u=s} = Q_u \cdot (M_u / M_u) \quad (1)$$

$${}_s Q_u = Q_{s0} \cdot \sqrt{1 - \eta_s^2} \quad (2)$$

$$Q_{s0} = \frac{2t(D-t) \cdot \sigma_{cy}}{\sqrt{3}} \quad (3)$$

$$\eta_s = N_s / N_y \quad (4)$$



where:  $Q_u$ : Maximum shear capacity in SC pile,  ${}_sQ_u$ : Steel contribution of maximum shear capacity in SC pile,  $M_u$ : Maximum moment capacity in SC pile,  ${}_sM_u$ : Steel contribution of maximum moment capacity in SC pile

## 2. Experimental program

### 2.1 Specimen details

Table 1 and Fig. 1 shows the elevation and cross section of the SC pile specimen (hereafter, SCS1) tested in the experiment. SCS1 has a 400mm outer diameter and 600mm height. The thickness of the steel casing is  $t_s=6$ mm and that of concrete is  $t_c=79.75$ mm. SCS1 was manufactured with a centrifugal casting concrete technique. Steel stub blocks were connected to the top and base region of the specimen with high tension bolts and the annular space between specimen and stub was filled with grout. A constant axial force of 1000kN in compression was applied to SCS1. The axial force ratio is about 0.10 based on total steel and concrete cross section areas. The shear span ratio was set at a small value, 0.75 of the outer diameter of the pile. Figure 2 shows a shear force (Q) and axial force (N) interaction curve (moment capacity was converted to shear force (Q) divided by shear span.). In this paper, the shear capacity of SCS1 was calculated by three equations, Case 1 to 3. Case 1 is Eq. (1) as shown above and listed in the 2000 BRI report. Case 2 is Eq. (5) and in this equation the concrete contribution of shear capacity is assumed to be given by the equation for Pretensioned spun high strength concrete piles (hereafter, PHC piles) based on a principal stress assumption [6] (the concrete shear contribution part is neglected for tensile axial force.). Case 3 is Eq. (2) which assumes only a steel contribution to shear capacity, that is, the concrete contribution is ignored. At the experimental axial force of 1000kN, shear capacity of Case1 ( $Q_1$ ), Case2 ( $Q_2$ ) and Case3 ( $Q_3$ ) are all less than the flexural capacity ( $Q_{bu\_fiber}$ ) calculated from a fiber model. Therefore, SCS1 was designed to fail in shear and the behavior was expected to be controlled by shear behavior.

Table 1 – Specimen details

Specimen	Outer diameter (mm)	Steel thickness, $t_s$ (mm)	Concrete thickness, $t_c$ (mm)	Height (mm)	Shear span (ratio) (mm)	Axial Force (ratio) (kN)
SCS1	400	6	79.75	600	300 (0.75)	+1000 (0.10)※

※ Positive is compression force.

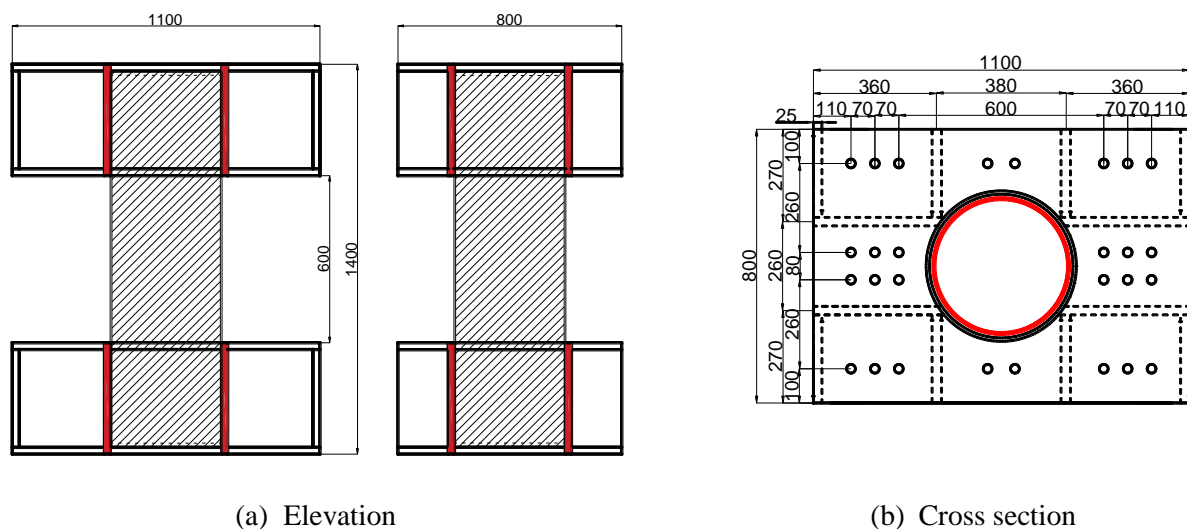


Fig. 1 – Elevation and cross section of SC pile specimen (Unit: mm)

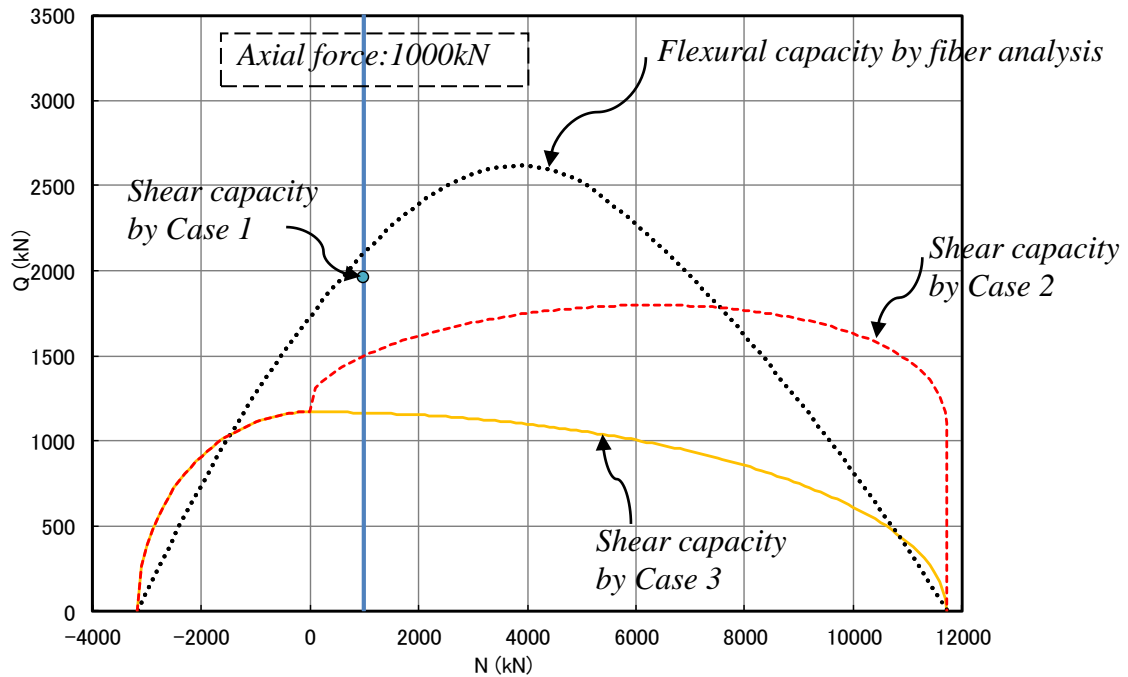


Fig. 2 – Shear capacity and axial force relation in SCS1

$$Q_u = Q_s + Q_c \quad (5)$$

$$Q_c = \alpha \cdot \eta_c \cdot \frac{t \cdot I}{S_o} \cdot \sqrt{(\sigma_g + 2\sigma_d)^2 - \sigma_g^2} \quad (6)$$

$Q_u$ : Maximum shear capacity in SC pile,  $Q_c$ : Concrete contribution of maximum shear capacity in SC pile,  $\alpha$ : Factor of shear span ratio,  $\eta_c$ : Reduction factor of scale effect,  $I$ : Inertial moment of concrete part,  $t$ : Thickness of concrete part,  $S_o$ : First inertial moment of concrete part,  $\sigma_g$ : prestressed stress,  $\sigma_d$ : Tensile stress of concrete

Table 2 shows the material mechanical properties used in the test. Concrete was tested with cylinders of 200mm diameter, 300mm height and 40mm thickness. The concrete had a high compressive strength, 110.6MPa. The steel casing was SKK490 grade steel.

Table 2 – Material mechanical properties

(a) Concrete			(b) Steel		
Compressive strength, $\sigma_m$ (MPa)	Compressive strain at $\sigma_m$ (%)	Young's modulus (MPa)	Yield strength, $\sigma_y$ ※ (MPa)	Strain at yield strength, $\epsilon_y$ ※ (%)	Young's modulus (MPa)
110.6	0.27	40300	428	0.414	200600

※ 0.2% offset yield strength and strain

## 2.2 Loading setup

Figure 3 shows the loading system. Horizontal force was applied with 3MN and 1.5MN hydraulic jacks. Axial force was kept constant at 1000kN and the upper stub block was kept parallel to the lower concrete block with two 4MN hydraulic jacks to realize nearly antisymmetric moment distribution. Load was applied



statically and the loading protocol was two cycles each at  $R=\pm 0.125\%$ ,  $\pm 0.25\%$ ,  $\pm 0.5\%$  and  $\pm 0.75\%$ . Then the specimen was loaded in the positive north direction to about  $+10\%$ . Loading was controlled by drift angle,  $R$ , which is the ratio of the relative horizontal displacement,  $\delta_h$ , to clear pile height,  $H=600\text{mm}$ .

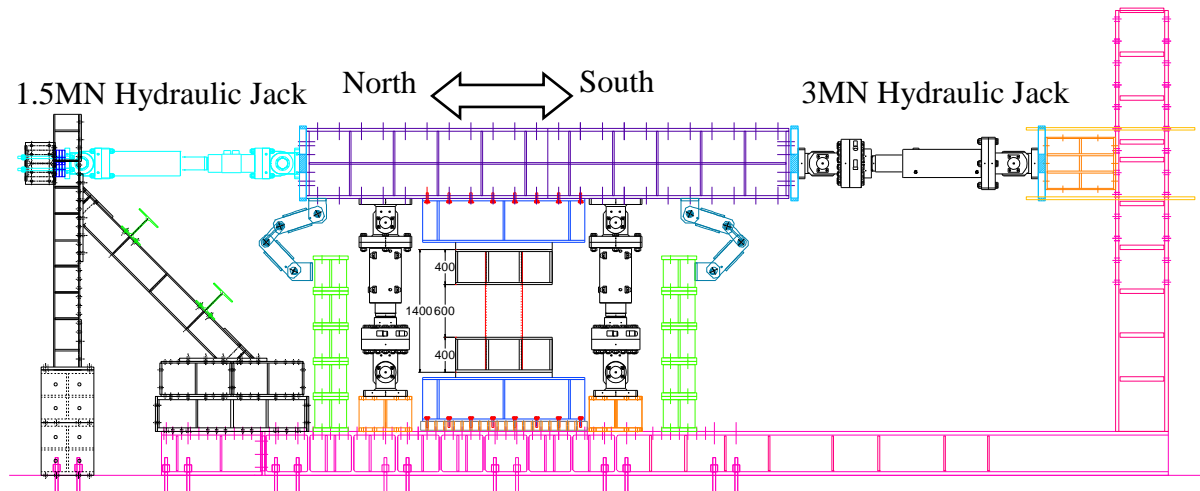


Fig. 3 – Loading system (Unit: mm)

### 3. Experimental results

#### 3.1 Shear force (Q) – Drift angle (R) relation

Figure 4 shows shear force (Q) and drift angle (R) relation. Five characteristic points are shown in this figure as well. These characteristic points include shear, tensile and compressive yielding of steel, as well as maximum capacity and ultimate capacity of the specimen. Ultimate capacity was defined as 20% degradation of lateral load capacity from the peak capacity. Figure 5 shows the position of rosette and uniaxial strain gauges installed on the outer surface of the steel casing. Shear yielding and tensile and compressive yielding of steel were judged by the rosette and uniaxial strain gauges. The reversed cycles up to 0.75% drift were applied with the 3MN hydraulic jack. Due to stability concerns, the loading was positive only to  $+10\%$ . In this loading, the 1.5MN jack was added to pull the specimen, which greatly limited out-of-plane movement.

SCS1 showed high shear force capacity and ductility in the experiment. It is observed that flexural yielding occurred in tension and compression at  $R=0.81\%$  and  $1.08\%$  at the top and bottom outer edge of the pile at first. The yield in shear of the steel casing occurred at  $R=1.14\%$  drift in the locations of sw2 and sw3. All position, sw1 to sw5 of the steel casing along the height yielded by  $R=1.6\%$  drift. After these events, maximum capacity was 2015kN at  $R=2.37\%$  drift with failure caused by local buckling of the steel casing at the top and bottom outer edge of the pile; the buckling was confirmed visually. This buckling occurred before the pile reached its high flexural moment capacity. Drift angle at ultimate capacity was about  $R=6.0\%$  drift. Final damage is shown in Fig. 6 after the end of loading. These photos show several shear cracks on the surface of concrete; however, the number of shear cracks and shear crack width were small. On the other hand, concrete crushing was observed at the top and bottom outer edge of the pile. Therefore, the failure mode of SCS1 was deemed to be due to flexure.

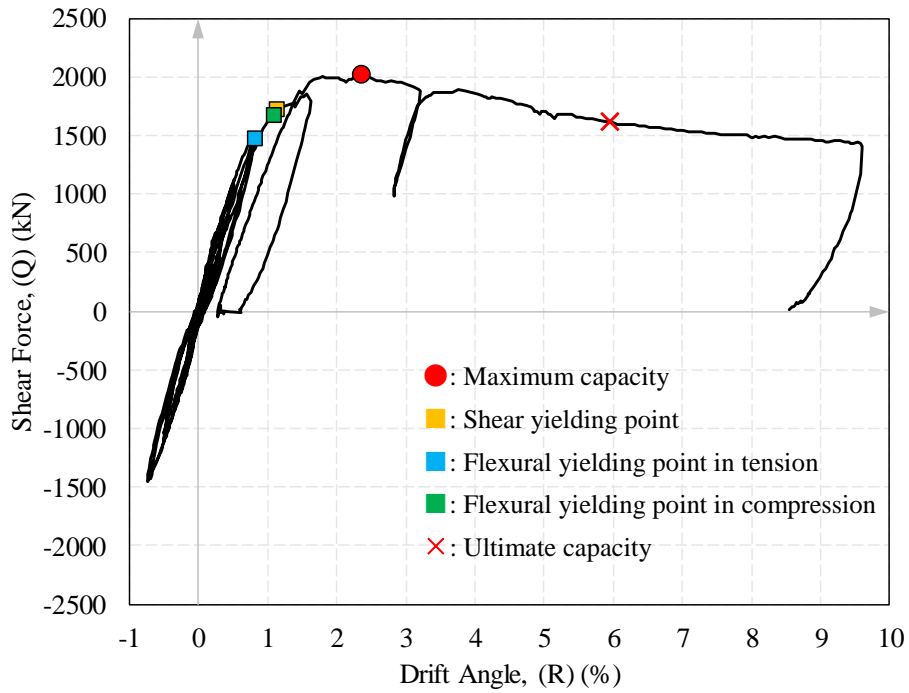


Fig. 4 – Shear force (Q) and drift angle (R) relation

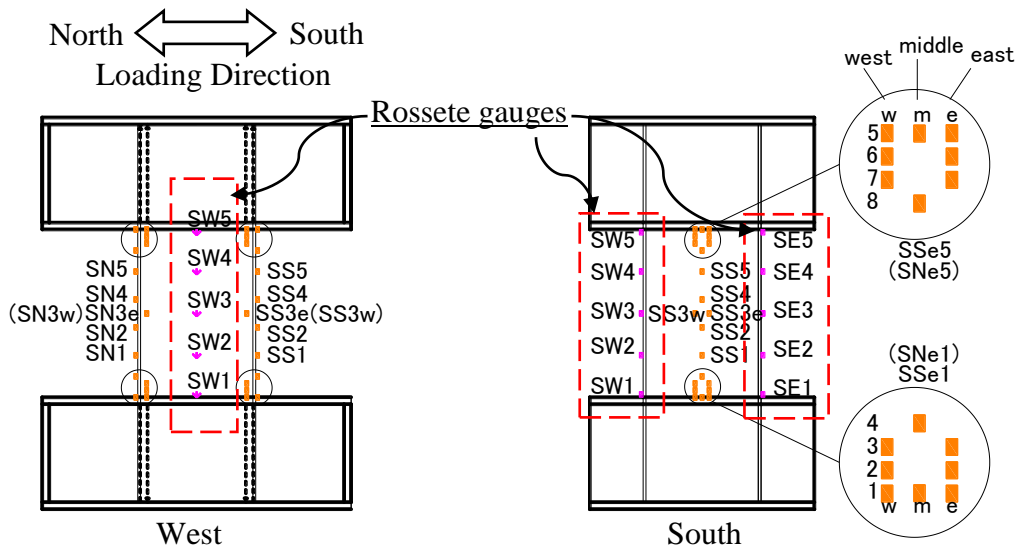


Fig. 5 – Location of strain gauges used in the test

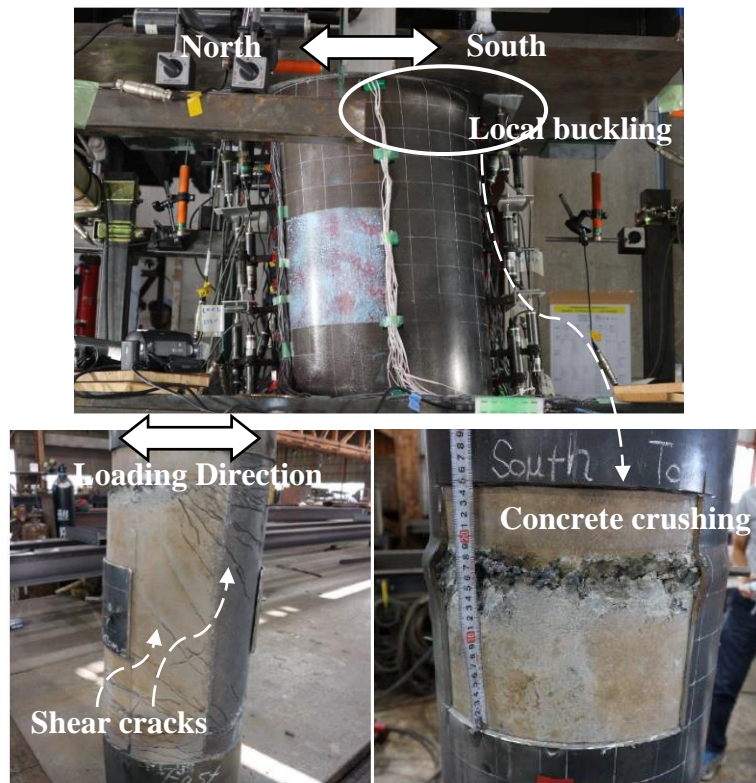


Fig. 6 – Observed damage after loading test

### 3.2 Comparison of maximum capacity with computation using equations

Table 3 shows a comparison of maximum capacity with computation results using Eq. (1) ( $Q_{su1}$ ), Eq. (5) ( $Q_{su2}$ ) and Eq. (2) ( $Q_{su3}$ ). In Table 3, flexural capacity based on fiber analysis,  $Q_{bu\_fiber}$  is also listed ( $Q_{bu\_fiber}$  does not take into account the effect of steel buckling.).

The computation of flexural capacity using the fiber model is in good agreement with maximum load capacity in the experiment. Shear capacity in the experiment was higher than the computation results under the current equations for shear maximum capacity. In Eq. (1) ( $Q_{su1}$ ), the ratio of experimental value to computed value was 1.11 and the shear capacity's contribution ratio of concrete component to steel component in Eq. (1) ( $Q_{su1}$ ) was 65%:35%. In Eq. (5) ( $Q_{su3}$ ), although the effect of concrete was considered in the principal stress theory, it also underestimated the experimental result because the concrete benefitted from the confining effect provided by the steel casing. The shear capacity's contribution ratio of concrete and steel components in Eq. (2) ( $Q_{su2}$ ) was 75%:25%. Eq. (3) ( $Q_{su3}$ ) considered only the steel component of the shear capacity and greatly underestimated the experimental results.

Table 3 – Comparison of maximum capacity with computation using Eq. (1) ( $Q_{su1}$ ), (2) ( $Q_{su2}$ ) and (5) ( $Q_{su3}$ )

<b>Specimen</b>	Exp. (kN)	$Q_{su1}$ (kN)	$Q_{su2}$ (kN)	$Q_{su3}$ (kN)	$Q_{bu\_fiber}$ (kN)	Exp./ $Q_{su1}$	Exp./ $Q_{su2}$	Exp./ $Q_{su3}$	Exp./ $Q_{bu\_fiber}$
SCS1	2015	1820	1530	1163	2046	1.11	1.32	1.73	0.985



## 4. Conclusions

SC pile specimen was tested to determine the shear maximum capacity of SC piles with small shear span ratios. Current equations were compared to experimental results to check their accuracy. The conclusions are summarized below.

- Flexural yielding of steel occurred before shear yielding of steel. Although shear yielding occurred before maximum capacity of the specimen, maximum capacity was likely governed by buckling of the steel casing.
- Experimental shear capacity was higher than the results from all existing shear capacity equations. Though both Eq. (1) and Eq. (5) evaluated shear capacity conservatively, the accuracy of these equations and the mechanism need much more investigation.
- Ignoring the concrete contribution to SC pile shear strength is unreasonably conservative.

## 5. Acknowledgements

This work was supported financially by the collaborative research project with Copita. It was also supported by JSPS through Grant-in-Aid program (PI: Susumu Kono). We are thankful to JST Program on Open Innovation Platform with Enterprises (JPMJOP1723), the Collaborative Research Project (Materials and Structures Laboratory), and the World Research Hub Initiative (Institute of Innovative Research), at Tokyo Institute of Technology for their generous support of this research.

## 6. References

References must be cited in the text in square brackets [1, 2], numbered according to the order in which they appear in the text, and listed at the end of the manuscript in a section called References, in the following format:

- [1] Architectural Institute of Japan (2014): Report on the Great East Japan earthquake Disaster, Joint Editorial Committee for the Report on the Great East Japan Earthquake Disaster.
- [2] Architectural Institute of Japan (2018): Report on the Damage Investigation of the 2016 Kumamoto Earthquakes.
- [3] Ikezaki D, Sako Y, Okano H (2018): Restoring Force Model for Prefabricated Concrete Piles, Journal of Structural and Construction Engineering (Transactions of AIJ), Architectural Institute of Japan
- [4] Building Research Institute (2019): Study on Structural Performance Evaluation for Concrete Pile Sub-assembly System with Post-earthquake Functional Use, Building Research Data
- [5] Building Research Institute (2000): Final Report on Seismic Performance of Pile and Pile Foundation
- [6] Architectural Institute of Japan (2017): AIJ Guidelines for Seismic Design of Reinforced Concrete Foundation Members (Draft)